Structure *14*, 1567–1576, October 2006 DOI 10.1016/j.str.2006.08.012

Ligand-Release Pathways in the Pheromone-Binding Protein of *Bombyx mori*

Frauke Gräter,[1] Bert L. de Groot,[1] Hualiang Jiang,[2] and Helmut Grubmüller[1,*]
[1] Department of Theoretical and Computational Biophysics
Max-Planck-Institute for Biophysical Chemistry
Am Fassberg 11
37077 Göttingen
Germany
[2] Drug Discovery and Design Center
Shanghai Institute of Materia Medica
Chinese Academy of Sciences
555 Zu Chong Zhi Road
Zhangjiang Hi-Tech Park
Shanghai 201203
China

Summary

Pheromone-binding proteins (PBP) supply olfactory neuron cells with pheromones by binding the ligands they are tailored for and carrying them to their receptor. The function of a PBP as an efficient carrier requires fast ligand uptake and release. The molecular basis of the ligand-binding mechanism was addressed here for the intriguing case of the PBP of the silk moth *Bombyx mori*. This PBP completely encapsulates its ligand bombykol without displaying any obvious ligand entrance/exit sites. Here, two opposite dissociation routes were identified as the most likely entrance/exit paths by replica-exchange molecular dynamics, essential dynamics, and force-probe molecular dynamics simulations. One of the paths runs along a flexible front lid; the other along the termini at the back. Calculated forces and energies suggest that both routes are physiologically relevant. The multiplicity of pathways may reduce or tune the entropic barrier for ligand binding.

Introduction

Olfactory systems of animals share general, yet largely unknown, mechanisms by which to achieve their required sensitivity and specificity. One of the common principles is the assistance of olfaction by odorant-binding proteins (OBPs), which are integral parts of the odorant signaling pathway and are restrictively expressed in olfactory tissues (Vogt and Riddiford, 1981; Pelosi et al., 1982). OBPs are nanocapsules that solubilize small hydrophobic molecules of the odorant blend by binding them into their central cavity (Steinbrecht et al., 1995; Tegoni et al., 2004). According to a current view, the odorant molecule is carried by the OBP to the neuronal membrane and is presented to the odorant receptor (OR) for receptor activation. For an OBP to function as a carrier and for it to play additional putative roles in odorant discrimination, receptor activation, and odorant deactivation, its uptake/release mechanisms need to be individually tuned (Steinbrecht, 1998). How this is achieved is yet to be elucidated.

The olfactory communication system of insects is an ideal model system for studying olfaction in molecular detail. The system is able to discriminate subtle differences in the chemistry of the small organic pheromone molecules, a special class of odorant molecules for sexual attraction (Karlson and Lüscher, 1959; Mori, 1998). In the well-studied case of the silk moth, *Bombyx mori*, the pheromone bombykol, produced and released by the female insect, is detected over large distances by the olfactory antennae of the male. As sketched in Figure 1A, the pheromone-binding protein from *Bombyx mori* (BmorPBP) acts as the transporter for bombykol through the sensillar lymph of the antennae to the pheromone receptor (Vogt and Riddiford, 1981; Kaissling, 2001; Sakurai et al., 2004).

Figures 1C and 1D show the crystal structure of bombykol-complexed BmorPBP, the first three-dimensional structure of an insect OPB solved (Sandler et al., 2000). The six α helices of PBP, stabilized by three interhelical disulphide bonds, form a rigid capsule with a mainly apolar core and a highly charged polar surface. Bombykol is completely enclosed within the hydrophobic cavity. Its hydroxyl group forms a hydrogen bond to one of the few internal polar residues, Ser56 (yellow in Figures 1C and 1D). Bombykol binding to BmorPBP is strong, with a 105 nM dissociation constant, K_D (Leal et al., 2005), at physiological pH. The NMR structure of uncomplexed BmorPBP shows a highly similar fold, with an empty, yet preformed, cavity to accommodate bombykol (Lee et al., 2002).

As for OBPs in general, a crucial, yet unsolved, question is the mechanism of ligand entrance and exit. Obviously, ligand uptake and release must be fast, i.e., it must occur within a millisecond timescale or faster to guarantee an equally fast nerve signal decay for sufficiently frequent readjustments of flight direction. Yet, as can be seen in Figure 1B, the protein conformation in the X-ray structure forms a tight envelope around bombykol without any obvious entrance/exit gates. To resolve this puzzle, we here address the question of which site of the BmorPBP structure provides a gate for efficient bombykol uptake and release. Apparently, the putative pathway requires a sufficiently low energetic barrier.

A first hint came from the fact that BmorPBP undergoes a conformational transition from the structure at neutral pH to an acidic fold at pH 4.5 (Wojtasek and Leal, 1999; Horst et al., 2001) with low binding affinity (Prestwich et al., 1995). Assuming that this pH-dependent conformational transition correlates with the ligand uptake and release mechanisms, two possible exit gates (blue in Figure 1C) have been suggested: (1) ligand passage along the front lid formed by residues 60–68, or (2) ligand passage along the N-terminal and C-terminal chains located at the back of BmorPBP, referred to below as the front and back pathway, respectively (Sandler et al., 2000; Horst et al., 2001). A previous molecular

*Correspondence: hgrubmu@gwdg.de

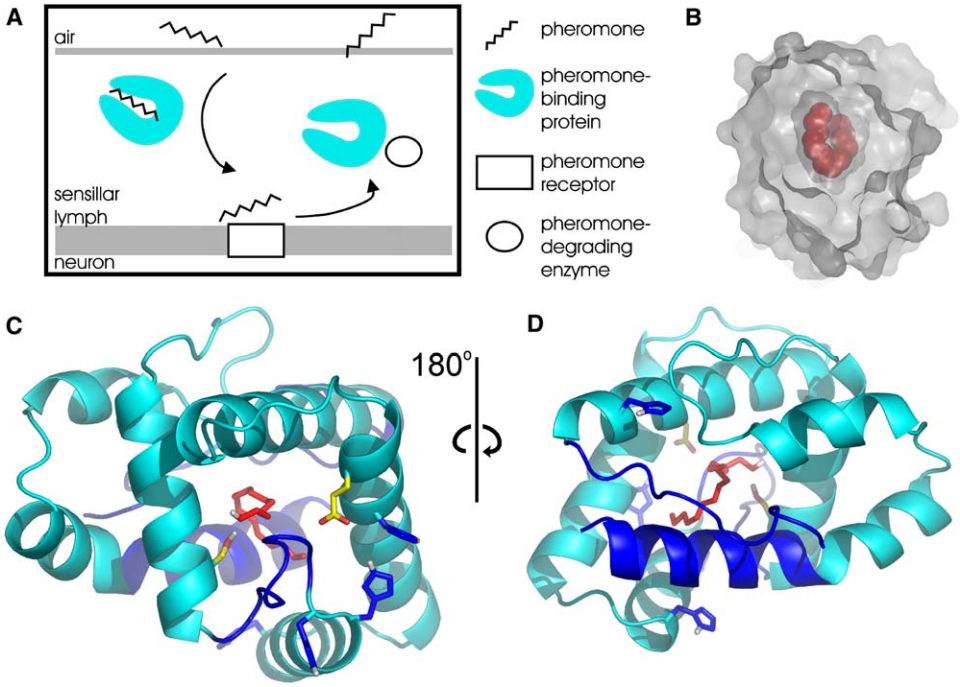

Figure 1. Olfactory System of *Bombyx mori*

(A) Pheromone reception involves the entrance of bombykol into the sensillar lymph, transport of bombykol by the pheromone-binding protein to the pheromone receptor, stimulation of the receptor by bombykol, and bombykol degradation.

(B) Bombykol (red spheres) is completely surrounded by its receptor, BmorPBP (gray surface).

(C and D) The bombykol-PBP complex (PDB code: 1DQE; Sandler et al., 2000) viewed from the front and back, respectively. Bombykol is shown in red, hydrogen bond partners Ser56 and Glu98 are shown in yellow, and His residues are shown as blue sticks. Regions presumably involved in ligand passage—the front lid (residues 60–68) and the terminal fractions (residues 1–14 and 126–137)—are colored blue. All proteins were plotted with Pymol (DeLano, 2001).

dynamics (MD) study (Nemoto et al., 2002) pointed, though only indirectly, to the front lid as the favored entrance and exit route of the ligand. Additional work with high-level ab initio calculations identified major interactions of BmorPBP side chains with bombykol in the bound state (Klusak et al., 2003). Here, we aim at a characterization of and the discrimination between the two putative ligand passage paths by means of MD simulations of the bombykol release from BmorPBP. To this end, the pathways for dissociation toward the front and back, as obtained from replica-exchange MD (Sugita and Okamoto, 1999; García and Sanbonmatsu, 2001), essential dynamics (ED) (Amadei et al., 1996; de Groot et al., 1996), and force-probe MD simulations (FPMD) (Grubmüller et al., 1996; Izrailev et al., 1997), were compared in terms of their mechanisms, forces, and energetics.

Results and Discussion

Dynamics of the Bound Complex

To obtain a first notion of putative pathways for ligand entrance and exit in BmorPBP, the BmorPBP and bombykol dynamics in the bound state were characterized. During the conventional 300 K MD simulations (50 ns, data shown elsewhere; Gräter et al., 2006), the terminal peptide fragments and the His-rich loop (residues 60–68) proved significantly more flexible than the otherwise rather rigid protein scaffold. This finding suggests that the front loop and the terminal fragments at the back are sufficiently flexible lids for ligand entrance and exit. Most notably, partial unbinding of bombykol toward the front lid involving an opening motion of the lid was observed. However, within the short nanoseconds timescale of our conventional MD simulations, the complex will not overcome larger energy barriers to other regions of the configurational space that are also sampled at physiological conditions. In particular, a role of the terminal fragments as possible second lids could not be excluded.

To enhance sampling, replica-exchange MD (REMD) simulations with increased temperatures were performed (Figure 2). With temperature steps of 80 K, exchange attempts of adjacent replicas were accepted with ratios of around 8%, due to a sufficient overlap of the potential energy distributions (Figure 2A). Thus, simulating all replicas with the same solvent temperature of 300 K resulted in a reasonable acceptance ratio at the desired temperature spacing in spite of the large system size. Figure 2B shows the exchange of a selected replicum within different temperatures (upper panel) and the consequent changes in rmsd of bombykol for two example temperatures (lower panel). The frequent exchanges enable bombykol to effectively sample the conformational space when bound to BmorPBP.

An outward movement of bombykol was observed, similar to the one seen in the 300 K MD simulations and also directed via the putative front lid toward the solvent. Figure 3A shows representative snapshots. This bombykol motion involved a transient rupture of

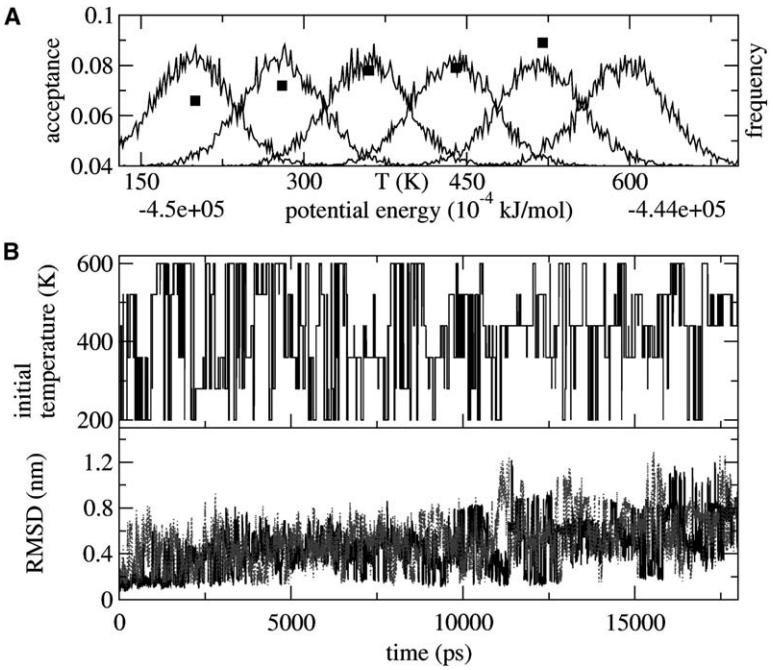

Figure 2. Results from Replica-Exchange Molecular Dynamics

(A) Potential energy distribution of the six replicas (black lines) and the acceptance ratio for the exchange of the replica at temperature T with the replica at temperature T + 80 K (squares).

(B) Efficiency of REMD for enhanced sampling. Upper panel: exchange of the replica with an initial temperature of 200 K between the six temperatures during REMD. Lower panel: rmsd of bombykol from the crystal structure of an example replica during REMD; the initial termperatures are indicated.

the bombykol-Ser56 hydrogen bond and the formation of hydrogen bonds to Glu98 and/or water and partial dislocation of the lid. Additionally, some REMD trajectories also showed a rotational motion of bombykol within the pocket and movements toward the back passageway near the protein termini, though to a smaller extent (Figure 3B).

The partial unbinding toward front and back was found to be represented by the same collective mode of fluctuation, specifically the first principal mode obtained from PCA, in opposite directions, respectively (Figure 3C). In both directions, conformations of extreme amplitude along the first eigenvector (EV) exhibited reduced protein-ligand interactions and increased solvent exposure of the ligand. This correlated motion of protein and ligand comprises both BmorPBP and bombykol dynamics, to which the protein with 87% of the total fluctuations substantially contributes.

This collective motion was further characterized by the curvilinear principal coordinate of the protein that optimally correlates to the ligand motion. It was calculated as suggested recently by Schröder et al. (Schröder, 2004; G. Schröder and H.G., unpublished data). Indeed, significant correlations were found,

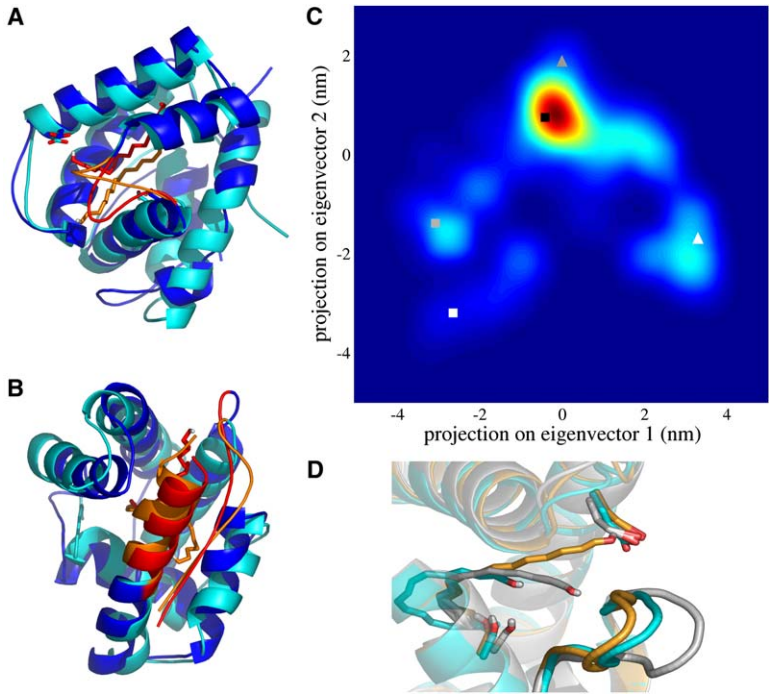

Figure 3. Principal-Component Analysis of the REMD

(A and B) Representative snapshots of the REMD simulation showing ligand release via the front and back, respectively. Bombykol and the parts of the protein serving as lids during release are shown in orange and red, respectively.

(C) Projection of the REMD trajectory onto the first two EVs. The first EV represents partial ligand release toward the front lid (high projection) and toward the termini at the back (low projection). Structures shown in (A) and (B) are shown as gray triangles (front) and squares (back), respectively; the crystal structure is shown as a black square.

(D) Correlation of protein and ligand dynamics. Representative structures along the nonlinear collective mode that best correlates to the ligand motion are shown. It exhibits a lid opening in conjunction with partial ligand dissociation toward the front.

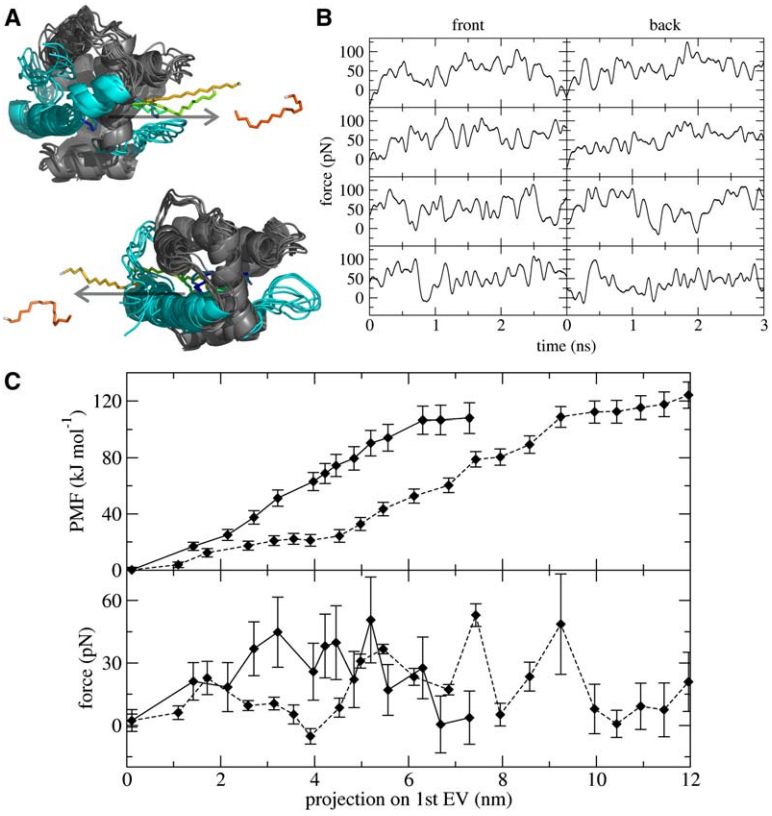

Figure 4. Ligand Release Probed by ED Simulations

(A) Snapshots during dissociation to the front (top) and the back (bottom) from one representative trajectory. Green, Yellow, Orange, bombykol; cyan, front loop and terminal helix and coil.

(B) Forces along the first EV to the front and back during four ED runs each.

(C) Extended sampling of forces at discrete positions along the first EV. PMF (upper panel) and forces (lower panel) along the dissociation toward the front (solid line) and back (dashed line), averaged over the last 2 ns of the sampling. Error bars indicate the standard deviation of averages over 0.2 ns windows.

most notably for the lid dynamics. Figure 3D shows representative snapshots of bombykol and the lid after projection onto the nonlinear mode of the largest amplitude. The mode represented an opening motion of the protein by a lid flip in conjunction with the ligand dynamics, to give way to the half-dissociated ligand.

Full unbinding, involving complete loss of protein-ligand interactions and the release of the entire ligand into water, was not observed, as it would presumably require further sampling and, hence, much longer simulation times.

Ligand-Release Pathways from Essential Dynamics

To further alleviate the sampling limitations, ED simulations were performed to study full ligand release. The REMD simulations revealed the first EV as a suitable reaction coordinate for the ligand motion toward the back and front exits. This EV therefore was chosen as the coordinate along which ED sampling in the positive (front exit) and negative (back exit) directions was carried out. By constraining the system to move along the first EV only in the defined direction, the system was forced to sample a much larger region of conformational space as compared to the free dynamics simulations. This indeed leads to ligand release toward the front and back, as can be seen from snapshots of example trajectories (Figure 4A). ED sampling along the second EV (Figure 3C), another mode of protein-ligand motion possibly involved in ligand binding and release, did not result in ligand release. As a measure for the barriers to ligand exit, the forces along the first EV were compared for the front and back exit paths as shown in Figure 4B. Unfortunately, as can be seen in the figure, the large fluctuations render it difficult to infer any significant preference for one or the other of the release pathways.

To resolve this problem, further MD simulations were carried out for fixed reaction coordinates along the two exit pathways. On the basis of the obtained forces and potentials of mean force (PMF), shown in Figure 4C, the exit of bombykol along the front and back lids is equally likely. Both pathways exhibit a rupture force of $\sim$30 ± 12 kJ mol^{-1} nm^{-1} (lower panel). The derived activation free energies of 108 and 124 ± 12 kJ mol^{-1}, respectively, for front and back release were also found to agree within the standard deviation (upper panel). Thus, still neither of the two sites is found to be preferred over the other, and, hence, both can serve as gates for bombykol release.

We note that the PMF overestimates the experimental dissociation free energy (42 kJ mol^{-1}; Leal et al., 2005) by more than a factor of two, likely due to insufficient sampling and nonequilibrium effects. In particular, the ensemble of the unbound ligand and protein is typically larger and is consequently sampled to a smaller extent than the bound state. Here, the accurate calculation of the dissociation free energy was presumably particularly complicated by the high degree of ligand conformational flexibility. Furthermore, the protein might be forced to undergo unfavorable conformational changes to permit ligand release that are irreversible on the timescale of the simulations and therefore misleadingly add to the calculated free energy difference. A nonoptimal reaction coordinate might be an additional reason for the present overestimation of the PMF. However, we here aimed at the difference between the two putative

pathways rather than at absolute binding free energies. Because the forces and free energies can be assumed to involve systematic deviations of the same size for both pathways (see Figure S1; see the Supplemental Data available with this article online), the difference is expected to be sufficiently more accurate than the absolute values.

As expected, since the ED rest upon the principal modes identified in the free dynamics of the bombykol-BmorPBP complex, the ligand was forced to proceed along those pathways to dissociate, to which the bound state dynamics already pointed at. More specifically, ligand release toward the front and back in all ED simulations involves conformations similar to the one shown in blue in Figures 3A and 3B.

Ligand-Release Pathways from Force-Probe Simulations

To probe a larger variety of ligand-release pathways and to reduce the bias introduced above by sampling along the first EV, as a third approach bombykol was pulled out of the cavity of BmorPBP by means of a pulling force in a predefined direction. Here, in contrast to the ED simulations described above, the protein was completely free to adapt to the exit motion of the ligand. In a first series of FPMD simulations, four different bombykol-BmorPBP conformations observed during the initial conventional MD simulations served as starting structures. The pulling directions were chosen such that the center of mass of bombykol was pulled toward the approximate center of the putative lid at the front and of the N- and C-terminal helix and tail at the back. Figure 5A shows these directions as solid arrows.

Figure 5B compares the force profiles obtained from FPMD simulations of the four starting structures. Respective intermediate conformations at the force maximum are shown in Figure 5C. For pulling toward the front, irrespective of the initial complex conformation, unbinding occurred via a transient Glu98-BOM hydrogen bond. Formation of this bombykol-BmorPBP hydrogen bond was accompanied by the rupture of the intramolecular Glu98-Leu68 hydrogen bond (Figures 5C and 5D), which clamps the front loop in complexed and vacant BmorPBP (Sandler et al., 2000; Lee et al., 2002). The front loop thereby transiently gained flexibility, allowed ligand passage, and, finally, is fixed again upon re-formation of the Glu98-Leu68 hydrogen bond. The semidissociated state, with the polar head of bombykol pointing partially out of the cavity, has been also observed in the REMD simulations (Figure 3). This state remained stable up to a force of ~300 pN. It is the final detachment of the hydrophobic ligand from the cavity, in particular from Trp110, that is directly located at the lid and its solvation with water that gave rise to the sudden force drop.

For bombykol release along the front lid, the mechanism and the involved forces are consistent with the findings obtained from sampling along the first EV by using ED (see above). Combining the results mentioned above, this suggests a well-defined pathway. In contrast, unbinding trajectories along the back pathway were found to be more diverse, which also points toward a larger entropic contribution to the unbinding free energy barrier, similar to that observed for antibody/antigen unbinding (Heymann and Grubmüller, 1999). The different starting structures yielded a variety of exit pathways close to the termini, even though bombykol was pulled toward the same direction. Since force peaks for

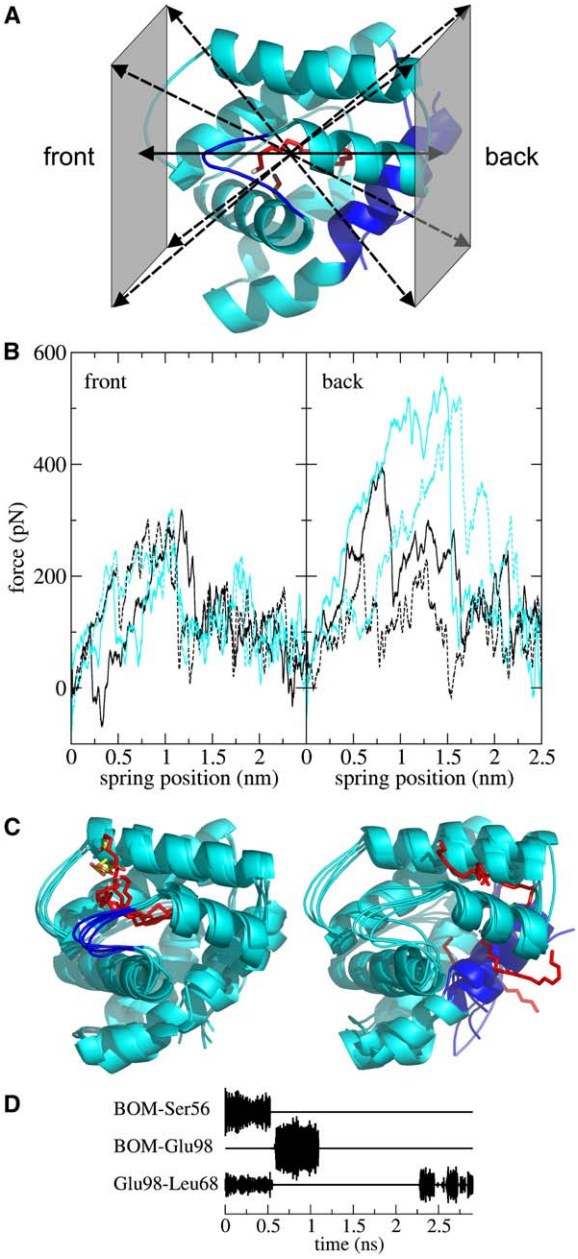

Figure 5. Ligand Release Probed by FPMD Simulations

(A) Chosen pulling directions.

(B) Force profiles from pulling toward the front lid (left panel) and the termini at the back (right panel) along the main pulling direction (solid arrows in [A]), obtained from four different trajectories each.

(C) Snapshots for which forces are maximal during force-induced unbinding along the main pulling direction. Pulling toward the front yields similar rupture forces and unbinding trajectories that have a transient hydrogen bond to Glu98 in common (left); pulling toward the back yields diverging forces and pathways (right). Red, bombykol; yellow, Glu98; blue, regions involved in ligand passage, including the front lid and the terminal fractions.

(D) Formation and rupture of hydrogen bonds involving the front loop (Glu98 and Leu68) during ligand release to the front.

backward unbinding scattered within ~100 pN, they did not allow for discrimination between unbinding toward the front and back on the basis of these few trajectories.

In order to elucidate the dependence of the trajectories and forces on the chosen pulling direction, for both putative exits, a second series of FPMD simulations with the aforementioned snapshots and, in addition, five different pulling directions (dashed and solid arrows in Figure 5A) were performed. Figure 6A compares the force profiles for the obtained ensemble of trajectories. For the release to the front and back, rupture forces scattered significantly (black lines in Figure 6A) and yield a slightly lower average for release toward the front exit (cyan lines).

In agreement with the FPMD simulations described above, front release exhibited a uniform mechanism in all cases. Independent of the chosen pulling direction, unbinding always proceeded along the front lid as described above. Rupture forces far beyond 300 pN were observed in those cases that required a relative rotation of protein and ligand to align the ligand and the lid direction with the pulling vector. If these directions initially differed, their alignment gave rise to additional friction, thus leading to an overestimation of the forces.

For back release, each of the five directions yielded a range of rupture forces and different release mechanisms. However, for two of them, strikingly lower forces were observed (Figure 6A, right panel). Interestingly, the underlying exit passageways of these two candidates, and only of these two, was in accordance with the pathway identified in the ED simulations. This pathway involved a turn of the bombykol molecule within the cavity, resulting in the formation of a transient bombykol-Ser9 hydrogen bond. The flexible C-terminal coil gave way for final ligand release. Trp37 here played a crucial role, as it constituted the endpoint of the hydrophobic bombykol-protein interaction during dissociation. The significantly lower rupture force and the consistency with the findings from ED sampling suggest that, among the ligand-release trajectories toward the back, this pathway is favored by bombykol.

Figure 6B shows a histogram of the rupture forces for bombykol dissociation to the front and back exits, binned into 40 pN intervals. We found that, on average, front pulling (~320 pN) required slightly lower forces than backward pulling (~450 pN). However, as discussed above, only part of the front and back pathway ensembles should be taken into account for this comparison, namely, the two trajectories of back release with the lowest rupture forces (Figure 6B, red) and those trajectories of front release with rupture forces of ~300 pN and less. With this in mind, a similar range of rupture forces was covered by these representatives.

The obtained work associated with ligand release to the front and back is compared in Figure 7. The two back release trajectories with the lowest rupture forces (right panel, red) arising from ligand dissociation in accordance with the ED simulation yielded work profiles similar in range to the work profiles obtained for front release (left panel). This confirms our earlier finding that neither of the two exits, front or back, can be excluded. We note that the calculated work inherently comprises nonequilibrium effects and hence is, as expected, on

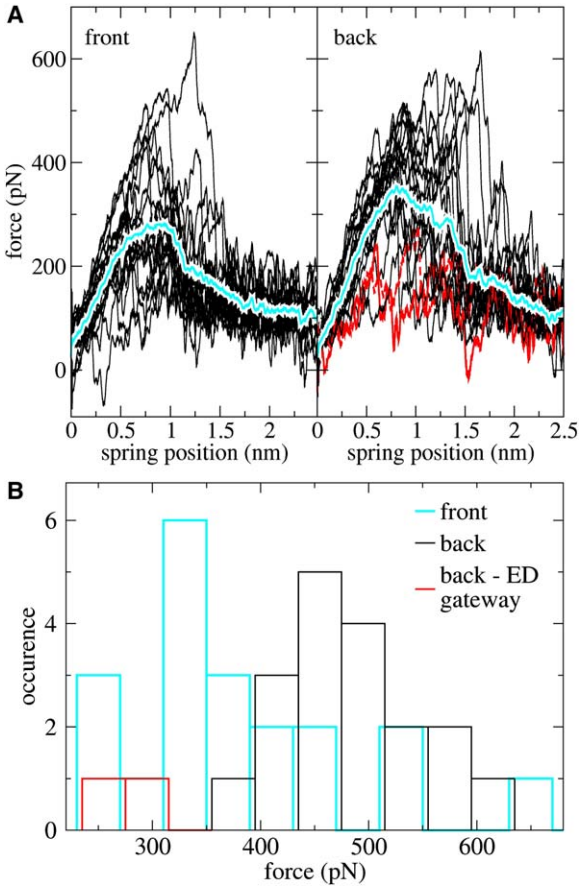

Figure 6. Ligand Release Probed by FPMD Simulations along Various Directions

(A) Force profiles from pulling toward the front (left panel) and back (right panel), each along five different directions (solid and dashed arrows in Figure 5A). The average over all 20 profiles is plotted in gray. The two profiles with mimimal rupture forces for back release are colored red.

(B) Histogram of rupture forces observed in FPMD simulations.

average, larger than the previously estimated PMF (Figure 4C) and the free energies derived from the work (see below).

An equality first formulated by Jarzynski permits the calculation of the PMF from an ensemble of nonequilibrium work profiles, provided sufficient sampling is available (Jarzynski, 1997; Hummer and Szabo, 2001). To allow its application, we performed a third set of FPMD simulations, now exclusively applying the previously identified prevalent pulling direction (solid arrows in Figure 5A). Since back release was not controllable by the pulling direction, and thus a prevalent direction could not be identified, the PMF could not be assessed for the back exit. As can be seen from the PMF derived for front release (cyan in Figure 7A), a free energy profile similar to the PMF from the ED simulation was obtained (Figure 4C), again with an overestimation of the dissociation free energy. The results for the PMF with cumulant expansion (Hummer, 2001; Park et al., 2003) (data not shown) turned out to be highly sensitive to the number of included trajectories, suggesting that the free energy estimate indeed is not yet sufficiently converged.

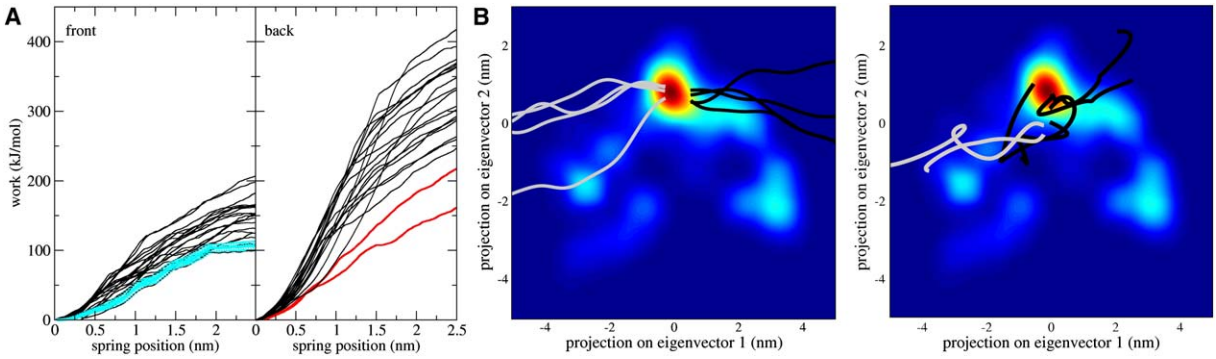

Figure 7. Free Energy Profile for Ligand Release from FPMD Simulations and Comparison of Release Pathways between FPMD and ED Simulations

(A) Work (black) and free energies (cyan) associated with ligand release toward the front and back calculated with the Jarzynski equation; red: preferred bombykol-release pathways to the back (as in Figure 6). The work was obtained from release toward the front along a single preferred direction and toward the back along different pulling directions and pathways.

(B) Comparison of protein/ligand motion during bombykol release obtained from ED (left panel) and FPMD (right panel). Trajectories were projected onto the EVs from REMD simulations (Figure 3). Gray, back release; black, front release.

A successful application of the Jarzynski equality would require larger ensembles of ligand-release trajectories or smaller pulling velocities, or both, to reduce nonequilibrium effects.

In summary, for the front exit, the ligand-release simulations suggested a unique mechanism along the putative front lid, for which indications were found also in the free dynamics of the bombykol-BmorPBP bound state. A half-dissociated state with a transient hydrogen bond from bombykol to BmorPBP and a detached front loop represents an intermediate. In contrast, numerous pathways were obtained for back release, among which a gate framed by the two termini could be identified as the most likely exit. Trp110 and Trp37, respectively, were identified as crucial residues stabilizing bombykol at the front and back exits just before its final release into the solvent. They thus can be assumed to lower the energy barrier for ligand binding and unbinding. Together with the residues forming transient hydrogen bonds to bombykol during release to the front and back, namely, Glu98 and Ser9, respectively, these residues are promising candidates for point mutations with the objective of testing our predictions and further exploring the two pathways.

Even though the ED and FPMD simulations are conceptually different, they share the course of the forces, PMFs, and the associated ligand/protein dynamics of the two identified exit gateways. This is also reflected by the projection of dissociation trajectories onto the first two EVs from REMD, as shown in Figure 7B. The motion along the first EV, as enforced in ED simulations (left panel), is reproduced in the pulling simulations for the back exit and to a certain extent for the front exit (right panel). In view of the significant contribution of protein fluctuations to the first EV, which were unbiased during the FPMD simulations, this is an astonishing agreement. The two different simulation methods by which to probe unbinding do not only yield similar ligand directions, but they also yield similar underlying protein main motion; they thus predict similar exit pathways. In the FPMD simulations, the front lid is detached from the neighboring helix only reversibly to temporarily give way to bombykol dissociation. Therefore, trajectories for front unbinding show only a transient motion to higher values of the first EV. The overall consistent picture strongly supports the identified opening lids, namely, the front His-rich loop and the terminal helix and coil with the respective intermediate states. The very similar barriers seen with the various methods suggest that both exit pathways are physiologically relevant.

Conclusion

The function of the olfactory protein BmorPBP as a carrier for its physiological binding partner, the pheromone bombykol, is closely linked to the mechanism and underlying energetics of bombykol uptake and release. Our simulations identified two ligand-release gateways, the front His-rich lid and a gateway framed by the terminal helix and coil. Both forces and free energies calculated for ligand release render the two pathways equally likely. Within an uncertainty in the relative free energy barriers of a few k_BT, we thus suggest that both pathways are indeed physiologically relevant. This conclusion rests on the results obtained from two different simulation techniques to enforce unbinding, ED and FPMD, which differ fundamentally in the reaction coordinate along which unbinding is enforced, an intrinsic mode of motion or an externally defined direction, respectively. The quantitative agreement of the mechanism and energetics obtained with the different approaches underscores our conclusion of two relevant ligand-release pathways.

Our simulations were challenged by the high conformational flexibility of the bound and unbound ligand. No preference of conformational states or pathways could be inferred from single trajectories and forces, which highly depended on the starting configuration and velocities. Therefore, extensive sampling was required in all cases. Besides its high biological relevance, the bombykol-BmorPBP system thus also represents a demanding, yet intriguing, test system for the calculation of binding free energies.

What might be the physiological purpose of two opposite pathways? The requirements for PBPs are in fact many-fold. Their function as carriers requires pheromone binding to be (1) tight to protect against degrading

proteins and to achieve a high pheromone sensitivity, (2) selective for serving as a prefilter with certain specificity in addition to the receptor, and (3) sufficiently fast (on a millisecond timescale) such that the kinetics of olfactory reception allows for a fast adjustment of the flight direction of the moth. Encapsulation of the entire ligand by an apparently impermeable protein envelope supports tight binding, but sterically impedes ligand entrance and exit by severely restricting the access to the cavity compared to solvent-exposed binding pockets. This particularly affects ligand uptake, which requires bombykol diffusion toward the entrance lid. BmorPBP exhibits a more or less uniformly negative electrostatic potential (data not shown) and a net charge of −8 at pH 7. Diffusion of bombykol, which is virtually apolar, toward its receptor BmorPBP hence is not directed by electrostatic funneling toward the entrance, as found for, e.g., acetylcholinesterase (Ripoll et al., 1993; Senapati et al., 2005), and thus may represent the rate-limiting step.

We therefore speculate that the physiological significance of two lids is to ensure a sufficiently fast rate of ligand uptake. By providing two pathways for bombykol entrance rather than one, the binding free energy barrier is lowered, and the area of access for bombykol to the BmorPBP cavity by random diffusion is enlarged. Electrostatic funneling, another way to ensure fast ligand binding and unbinding, enables acetylcholinesterase to rapidly take up and release *different* molecules, namely, the substrate and products, via two (or more) opposite one-way gates (Ripoll et al., 1993). Here, for the carrier protein at hand, fast binding and unbinding of the *same* molecule, instead, is achieved by two nondirectional pathways.

Furthermore, two alternative pathways warrant robustness of the binding properties of BmorPBP against point mutations that eliminate one of the routes. The previous finding that mutating Trp37, a residue located at the back gateway, leaves the binding energetics and kinetics unchanged, was unexpected (Leal et al., 2005), since this residue, conserved in most PBPs, is thought to be physiologically important. Now, in light of the two-pathway model, this robust behavior of BmorPBP toward mutation at only one of the pathways is explained. Accordingly, we suggest that double mutations at both pathways affect the binding kinetics.

In conclusion, the two identified discrete pathways to a central cavity provide the moth with the advantage of facilitating ligand entrance and exit without the loss of binding affinity and selectivity. This hypothesis can in principle be validated experimentally by point mutations. Potential candidates, as discussed above, are mutations of Trp37 and Trp110 to, e.g., alanine, which are expected to eliminate the stabilizing influence of the Trp-bombykol hydrophobic interactions onto the half-dissociated intermediate state. Alternatively, a complete steric blockage of the gates might be achieved by fixing the opening lids of the exit gates by disulphide bonds. The temporary hydrogen bond partners of bombykol during dissociation, Glu98 at the front and Ser9 at the back, together with an appropriate proximal bonding partner, are also suitable for this purpose. The 4-fold cysteine mutation should result in a substantial hindrance of bombykol uptake.

If our model of two relevant pathways is correct, one would expect a substantial change of the binding affinity and kinetics only if *both* pathways are eliminated by point mutations. A mutation at only *one* of the exits, instead, should alter the binding kinetics and energetics only by lowering the uptake rate due to the diffusional effect discussed above. Together, this suggests a rigorous test for our two-pathway model.

We here aimed at elucidating the pathway for bombykol uptake and release at neutral pH, at which bombykol is taken up on a millisecond timescale (Leal et al., 2005), but released significantly more slowly. Under physiological conditions, fast release of bombykol has been suggested to be triggered by a pH change (Wojtasek and Leal, 1999; Horst et al., 2001). Thus, the important questions to address next are how BmorPBP undergoes the conformational transition toward its acidic low-affinity structure and at what point this transition induces ligand release. This will be addressed in further investigations.

Experimental Procedures

MD and Replica-Exchange MD Simulations

The simulation setup and force field for BmorPBP and bombykol (PDB code: 1DQE; Sandler et al., 2000, chain A) are described elsewhere (Gräter et al., 2006). Equilibrated configurations were subjected to the subsequent replica-exchange MD (REMD), force-probe MD (FPMD), and essential dynamics (ED) simulations.

REMD simulations (Sugita and Okamoto, 1999; García and Sanbonmatsu, 2001; Sanbonmatsu and García, 2002) with six replicas, each 18 ns in length, have been performed. Simulated temperatures were 200, 280, 360, 440, 540, and 600 K. BmorPBP and bombykol were coupled to a heat bath at the respective temperature, whereas solvent and ions were coupled independently to a 300 K heat bath, with a coupling time of τ_T = 0.1 ps (Berendsen et al., 1984). In this way, the number of degrees of freedom of the system adding to the difference of potential energies of two replicas was reduced. This narrows the energy distributions, i.e., increases their overlap, and thus results in a reasonable acceptance ratio of ~8% at the desired temperature spacing, in spite of the large system size. Exchanges of configurations were attempted every 2 ps.

Essential Dynamics and Force-Probe MD Simulations

Along the first eigenvector (EV) obtained from the principal-component analysis (García, 1992; Amadei et al., 1993; Grubmüller et al., 1995) of the REMD trajectory, ED simulations (Amadei et al., 1996; de Groot et al., 1996) were performed. At each simulation step, the system was forced to increase or keep the distance to its starting position along the first EV, while the other degrees of freedom were unperturbed. The maximal step size along the EV was restricted to 10^{-5} nm/step to ensure that the system proceeds slowly enough to allow equilibration of the remaining degrees of freedom.

Two ED simulations were carried out. For the first, unbinding toward the front lid was enforced by increasing the position along the first EV; for the second, unbinding toward the back was enforced by decreasing the position. To enable the estimation of a potential of mean force (PMF), sampling of forces during the ED simulations was improved by carrying out additional MD simulations at equidistant points along the first EV. To this end, a total of 34 snapshots of the 2 ED trajectories were taken as starting structures for simulations of 6 ns each. During each of these simulations, the position on the first EV was kept fixed and the other degrees of freedom were equilibrated. Constraint forces, acting on the first EV, were recorded every 100 MD steps, allowing for the reconstruction of a PMF. Convergence of forces and free energies was carefully monitored.

As starting structures for the FPMD simulations, four snapshots were taken from the initial equilibration phase. For each of the snapshots, the system size was increased by adding water and ions at the side to which bombykol was pulled out of the cavity such that the box could accommodate the dissociated protein and ligand, yielding box dimensions of ~7.1 × 6.7 × 8.1 nm^3, containing

~38,000 atoms. Additional water molecules and ions were equilibrated during a 100 ps MD simulation with positional constraints on the protein and ligand as described above. In subsequent FPMD simulations, the center of mass of bombykol was subjected to a harmonic spring potential, which was moved along the pulling direction with a constant velocity of 1 m/s, as described previously (Grubmüller et al., 1996; Gräter et al., 2005). The force constant of the spring was set to 500 kJ mol^{-1} nm^{-2}. Simulations with ten different pulling directions were performed, starting from the four snapshots. As indicated in Figure 5A, one pulling vector was chosen such that it points directly toward the front and back pathways. The others were chosen to form an angle of 55° with respect to this vector. The center of mass of the protein was fixed to prevent the protein from being dragged by the ligand motion. Forces were recorded at each MD step and smoothened with a Gaussian filter of 1.6 Å width (Gräter et al., 2005).

Supplemental Data

The examination of the PMF convergence during ED sampling and movies of bombykol unbinding along the front and back exits obtained from FPMD simulations are available at http://www.structure.org/cgi/content/full/14/10/1567/DC1/.

Acknowledgments

We thank Karl-Ernst Kaissling for pointing out the pheromone-binding protein of *Bombyx mori* to us. We also thank him and Walter Leal for stimulating discussions and for carefully reading the manuscript. This work was supported by Volkswagen Foundation grants I/78 420 and I/80 585 (to H.G.) and a PhD scholarship of the Boehringer Ingelheim Fonds (to F.G.). We also acknowledge financial support from the 863 Hi-Tech Program of China (H.J., grant 2002AA104270).

Received: June 19, 2006
Revised: July 25, 2006
Accepted: August 2, 2006
Published: October 10, 2006

References

Amadei, A., Linssen, A.B.M., and Berendsen, H.J.C. (1993). Essential dynamics of proteins. Proteins *17*, 412–425.

Amadei, A., Linssen, A.B.M., de Groot, B.L., van Aalten, D.M.F., and Berendsen, H.J.C. (1996). An efficient method for sampling the essential sub-space of proteins. J. Biomol. Struct. Dyn. *13*, 615–626.

Berendsen, H.J.C., Postma, J.P.M., van Gunsteren, W.F., Nola, A.D., and Haak, J.R. (1984). Molecular dynamics with coupling to an external bath. J. Chem. Phys. *81*, 3684–3690.

de Groot, B.L., Amadei, A., van Aalten, D.M.F., and Berendsen, H.J.C. (1996). Towards an exhaustive sampling of the configurational spaces of the two forms of the peptide hormone guanylin. J. Biomol. Struct. Dyn. *13*, 615–626.

DeLano, W.L. (2001). PyMOL Manual (http://www.delanoscientific.com).

García, A.E. (1992). Large-amplitude nonlinear motions in proteins. Phys. Rev. Lett. *68*, 2696–2699.

García, A.E., and Sanbonmatsu, K.Y. (2001). Exploring the energy landscape of a β hairpin in explicit solvent. Proteins *42*, 345–354.

Gräter, F., Shen, J.H., Jiang, H.L., Gautel, M., and Grubmüller, H. (2005). Mechanically induced titin kinase activation studied by force-probe molecular dynamics simulations. Biophys. J. *88*, 790–804.

Gräter, F., Xu, W., Leal, W., and Grubmüller, H. (2006). Pheromone discrimination by the pheromone-binding protein of *Bombyx mori*. Structure *14*, this issue, 1577–1586.

Grubmüller, H., Ehrenhofer, N., and Tavan, P. (1995). Conformational dynamics of proteins: Beyond the nanosecond time scale. In Proceedings of the Workshop 'Nonlinear Excitations in Biomolecules,' May 30–June 4, 1994, Les Houches (France). M. Peyard, ed., 231–240. Centre de Physique des Houches (France), Springer-Verlag.

Grubmüller, H., Heymann, B., and Tavan, P. (1996). Ligand binding: molecular mechanics calculation of the streptavidin-biotin rupture force. Science *271*, 997–999.

Heymann, B., and Grubmüller, H. (1999). AN02/DNP unbinding forces studied by molecular dynamics AFM simulations. Chem. Phys. Lett. *303*, 1–9.

Horst, R., Damberger, F., Luginbuhl, P., Guntert, P., Peng, G., Nikonova, L., Leal, W.S., and Wuthrich, K. (2001). NMR structure reveals intramolecular regulation mechanism for pheromone binding and release. Proc. Natl. Acad. Sci. USA *98*, 14374–14379.

Hummer, G. (2001). Fast-growth thermodynamic integration: error and efficiency analysis. J. Chem. Phys. *114*, 7330–7337.

Hummer, G., and Szabo, A. (2001). Free energy reconstruction from nonequilibrium single-molecule pulling experiments. Proc. Natl. Acad. Sci. USA *98*, 3658–3661.

Izrailev, S., Stepaniants, S., Balsera, M., Oono, Y., and Schulten, K. (1997). Molecular dynamics study of unbinding of the avidin-biotin complex. Biophys. J. *72*, 1568–1581.

Jarzynski, C. (1997). Nonequilibrium equality for free energy differences. Phys. Rev. Lett. *78*, 2690–2693.

Kaissling, K.E. (2001). Olfactory perireceptor and receptor events in moths: a kinetic model. Chem. Senses *26*, 125–150.

Karlson, O., and Lüscher, M. (1959). Pheromones: A new term for a class of biologically active substance. Nature *183*, 55–56.

Klusak, V., Havlas, Z., Rulisek, L., Vondrasek, J., and Svatos, A. (2003). Sexual attraction in the silkworm moth: nature of binding of bombykol in pheromone binding protein—an ab initio study. Chem. Biol. *10*, 331–340.

Leal, W.S., Chen, A.M., Ishida, Y., Chiang, V.P., Erickson, M.L., Morgan, T.I., and Tsuruda, J.M. (2005). Kinetics and molecular properties of pheromone binding and release. Proc. Natl. Acad. Sci. USA *102*, 5386–5391.

Lee, D., Damberger, F.F., Peng, G.H., Horst, R., Guntert, P., Nikonova, L., Leal, W.S., and Wuthrich, K. (2002). NMR structure of the unliganded *Bombyx mori* pheromone-binding protein at physiological pH. FEBS Lett. *531*, 314–318.

Mori, K. (1998). Chirality and insect pheromones. Chirality *10*, 578–586.

Nemoto, T., Uebayashi, M., and Komeiji, Y. (2002). Flexibility of a loop in a pheromone binding protein from Bombyx mori: a molecular dynamics simulation. Chem.-Bio. Inf. J. *2*, 32–37.

Park, S., Khalili-Araghi, F., Tajkhorshid, E., and Schulten, K. (2003). Free energy calculation from steered molecular dynamics simulations using Jarzynski's equality. J. Chem. Phys. *119*, 3559–3566.

Pelosi, P., Baldaccini, N.E., and Pisanelli, A.M. (1982). Identification of a specific olfactory receptor for 2-isobutyl-3-methoxypyrazine. Biochem. J. *201*, 245–248.

Prestwich, G.D., Du, G.H., and Laforest, S. (1995). How is pheromone specificity encoded in proteins. Chem. Senses *20*, 461–469.

Ripoll, D.R., Faerman, C.H., Axelsen, P.H., Silman, I., and Sussman, J.L. (1993). An electrostatic mechanism for substrate guidance down the aromatic gorge of acetylcholinesterase. Proc. Natl. Acad. Sci. USA *90*, 5128–5132.

Sakurai, T., Nakagawa, T., Mitsuno, H., Mori, H., Endo, Y., Tanoue, S., Yasukochi, Y., Touhara, K., and Nishioka, T. (2004). Identification and functional characterization of a sex pheromone receptor in the silkmoth *Bombyx mori*. Proc. Natl. Acad. Sci. USA *101*, 16653–16658.

Sanbonmatsu, K.Y., and García, A.E. (2002). Structure of met-enkephalin in explicit aqueous solution using replica exchange molecular dynamics. Proteins *46*, 225–234.

Sandler, B.H., Nikonova, L., Leal, W.S., and Clardy, J. (2000). Sexual attraction in the silkworm moth: structure of the pheromone-binding-protein-bombykol complex. Chem. Biol. *7*, 143–151.

Schröder, G. (2004). Simulation of fluorescence spectroscopy experiments. PhD thesis, University of Göttingen, Göttingen, Germany.

Senapati, S., Bui, J.M., and McCammon, J.A. (2005). Induced fit in mouse acetylcholinesterase upon binding a femtomolar inhibitor: a molecular dynamics study. J. Med. Chem. *48*, 8155–8162.

Steinbrecht, R.A. (1998). Odorant-binding proteins: expression and function. Olfaction and Taste XII *855*, 323–332.

Steinbrecht, R.A., Laue, M., and Ziegelberger, G. (1995). Immunolocalization of insect odorant-binding proteins—a comparative-study. Chem. Senses *20*, 109–110.

Sugita, Y., and Okamoto, Y. (1999). Replica-exchange molecular dynamics method for protein folding. Chem. Phys. Lett. *314*, 141–151.

Tegoni, M., Campanacci, V., and Cambillau, C. (2004). Structural aspects of sexual attraction and chemical communication in insects. Trends Biochem. Sci. *29*, 257–264.

Vogt, R.G., and Riddiford, L.M. (1981). Pheromone binding inactivation by moth antennae. Nature *293*, 161–163.

Wojtasek, H., and Leal, W.S. (1999). Conformational change in the pheromone-binding protein from *Bombyx mori* induced by pH and by interaction with membranes. J. Biol. Chem. *274*, 30950–30956.